Chapter 13

Application of PLD-Fabricated Thick-Film Permanent Magnets

Masaki Nakano, Takeshi Yanai and
Hirotoshi Fukunaga

Additional information is available at the end of the chapter

http://dx.doi.org/10.5772/64235

Abstract

Isotropic Nd-Fe-B thick-film magnets have been prepared using a pulsed laser deposition (PLD) method with the control of laser energy density (LED) followed by post-annealing. The characteristics of the method are a high deposition rate up to several tens of microns per hour together with a reliability of magnetic properties due to the good transfer of composition from an Nd-Fe-B target to a film. Several micro-machines comprising the isotropic Nd-Fe-B films such as a miniaturized DC motor and a swimming machine in liquid were demonstrated. Furthermore, the deposition of isotropic Nd (or Pr)-Fe-B thick-film magnets on a Si or glass substrate was carried out to apply the films to various micro-electro-mechanical-systems (MEMS). We also introduced the preparation of isotropic Sm-Co, Fe-Pt, and nano-composite Nd-Fe-B+α-Fe film magnets synthesized using the PLD.

Keywords: pulsed laser deposition, thick-film magnet, isotropic, post-annealing

1. Introduction

Much research on anisotropic Nd-Fe-B film magnets thicker than several microns was carried out in order to advance miniaturized electronic devices including micro-electro-mechanical-systems (MEMS) [1–7]. It is generally known that the $(BH)_{max}$ value of an isotropic Nd-Fe-B film [8, 9] is smaller than that of an anisotropic Nd-Fe-B one; however, the flexibility of magnetization of the isotropic films is attractive in practical and various applications. Töpfer et al. demonstrated a multipolarly magnetized isotropic Nd-Fe-B film using a screen printing method

[10]. Yamashita et al. also reported that the torque of a milli-size motor comprising a multipolarly magnetized isotropic thick film exceeded the torque of a motor using an anisotropic one [11].

In Sm-Co thick-film magnets, we have difficulty in overcoming the values of $(BH)_{max}$ for Nd-Fe-B films due to the low saturation magnetization. However, several researchers have demonstrated Sm-Co thick films because of their high Curie temperature and good corrosion resistance [12–19]. For example, Cadieu et al. reported in-plane anisotropic Sm-Co films with a thickness above 100 μm using sputtering together with pulsed laser deposition (PLD) methods [16, 17]. In addition, Budde and Gatzen demonstrated a magnetic micro-actuator comprising a sputtering-made 30-μm-thick Sm-Co film [19].

Fe-Pt magnet is a promising material to use in the medical field owing to its outstanding biocompatibility [20]. In order to advance medical MEMS, the miniaturization of Fe-Pt magnets is necessary [21]. Aoyama and Honkura [22] and Liu et al. [23] reported isotropic Fe-Pt film magnets thicker than several microns using a sputtering method from the medical application point of view.

Here, we show the properties of isotropic Nd-Fe-B [24–28] thick-film magnets prepared using the PLD method and several miniaturized machines [24, 25, 28] comprising the Nd-Fe-B thick film. Moreover, PLD-fabricated isotropic Sm-Co, Fe-Pt, and nano-composite Nd-Fe-B+α-Fe thick films were introduced.

2. Experimental

A target such as Nd-Fe-B, Pr-Fe-B, Sm-Co, and Fe-Pt was ablated with an Nd-YAG pulse laser with a wavelength of 355 nm together with a frequency of 30 Hz in a vacuum atmosphere. The chamber was evacuated to approximately 4×10^{-5} Pa with a vacuum equipment before the deposition. During the deposition, each target was rotated and the distance between the target and the substrate (*T-S* distance) varied from 5 to 20 mm. In the experiment, a laser power was measured with a power meter in front of the entrance lens of the chamber. The laser energy density (LED) varied by controlling the laser power (LP) together with a spot size of laser beam which could be changed by moving the distance between the focal lens and the target intentionally (see **Figure 1**). Here, the spot size was expressed as a defocusing rate (DF rate) = (TD − FD)/FD × 100(%), where TD is the distance between the condensing lens and the target and FD is the focal length. In the experiment, the control of the defocusing rate (DF rate) enabled us to change LED widely compared with the variation of LP.

In some experiments, the post-annealing of a conventional annealing (CA) and a pulse annealing (PA), respectively, was carried out as shown in **Figure 2**. After magnetizing each sample up to 7 T with a pulse magnetizer, M-H loops were measured by using a vibrating sample magnetometer (VSM) which could apply a magnetic field up to approximately 1800 kA/m reversibly. The average thickness was mainly measured with a micrometer. In some samples, the thickness was estimated from hysteresis loops of as-deposited films [29]. Surface observation and composition analysis were carried out by using a scanning electron microscope (SEM) and an SEM-energy-dispersive X-ray spectroscopy (EDX), respectively.

http://dx.doi.org/10.5772/64235

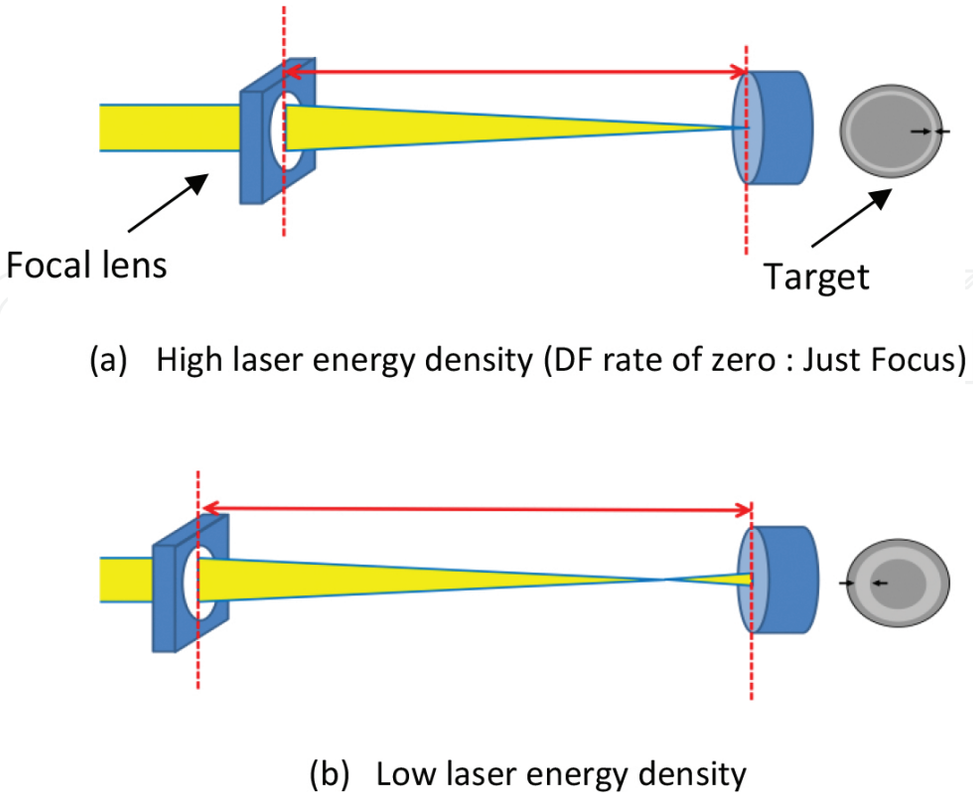

Figure 1. Schematic diagrams of deposition process with several values of the laser energy density (LED) which was controlled by changing the laser power and DF rate independently. (a) High laser energy density (DF rate of zero: just focus) and (b) low laser energy density.

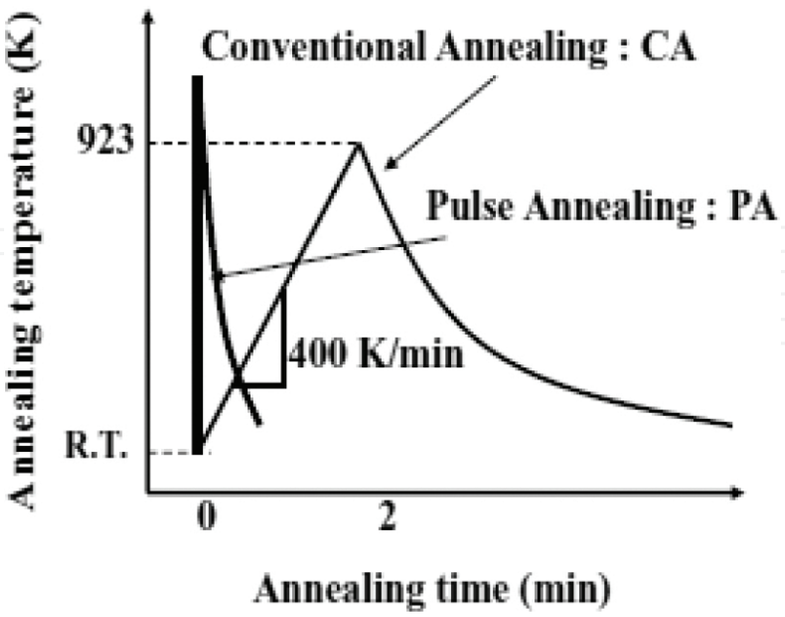

Figure 2. Schematic diagram of conventional annealing (CA) and pulse annealing (PA) methods.

3. Results

3.1. PLD-fabricated isotropic Nd-Fe-B thick-film magnets

Figure 3 shows the in-plane demagnetization curves of isotropic Nd-Fe-B thick-film magnets after the crystallization using two methods of CA and PA with each optimum condition. Both samples were prepared using an $Nd_{2.4}Fe_{14}B$ target under the deposition rate higher than 40 μm/h. The annealing duration of PA was approximately 1.8 s and the ramping rate of CA was 400 K/min (see **Figure 2**). The coercivity value of the annealed film using PA method was larger by approximately 300 kA/m than the annealed 673 K/min sample using CA method. On the other hand, the remanence and $(BH)_{max}$ values of the two samples were almost the same. Transmission electron microscopy (TEM) observation revealed that the use of PA method enabled us to reduce the size of $Nd_2Fe_{14}B$ grains compared with that of the sample annealed using CA method. We considered that the enhancement in coercivity is due to the increases in the domain pinning sites. From these results, a high-speed crystallization annealing process (PA method) is a promising method to refine $Nd_2Fe_{14}B$ grains of PLD-fabricated Nd-Fe-B thick-film magnets.

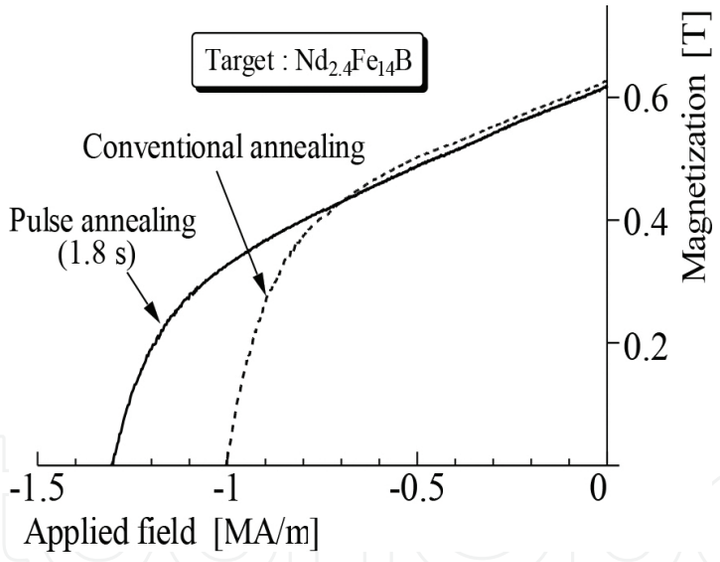

Figure 3. Demagnetization curves (in-plane) of PLD-made Nd-Fe-B thick films crystallized by two methods of CA and PA.

Figure 4 shows the relationship between the LED and magnetic properties of annealed Nd-Fe-B film magnets deposited on Ta substrates prepared using an $Nd_{2.6}Fe_{14}B$ target. All the samples were annealed using PA method. As the inset in each figure shows, the laser power LP and DF rate were controlled independently. In low energy density, high coercivity (H_c) and low remanence (M_r) were obtained, respectively. The samples with low H_c and high M_r were prepared in high energy density. In order to obtain the high deposition rate above 40 μm/h, LED less than 30 mJ/mm^2 was used. In this chapter, PA method was used in the results of

http://dx.doi.org/10.5772/64235

Sections 3.1–3.5. On the other hand, energy density above 200 mJ/mm^2 was used in the results of Sections 3.5 and 3.6.

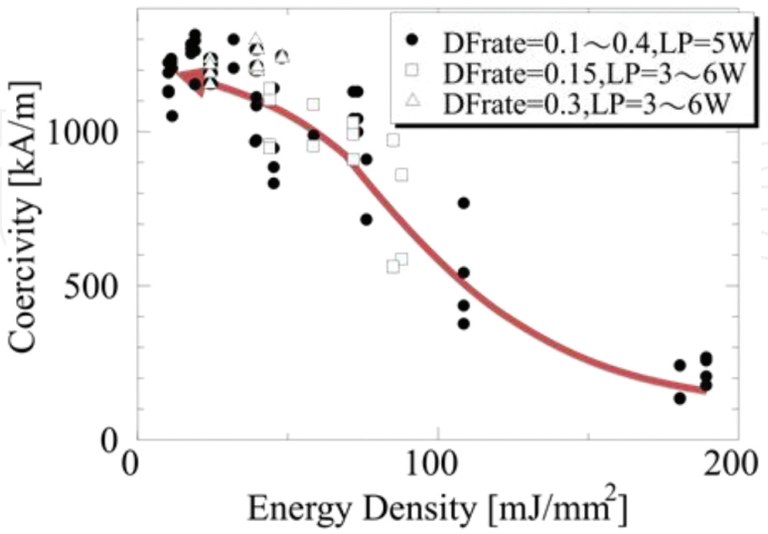

(a) Coercivity

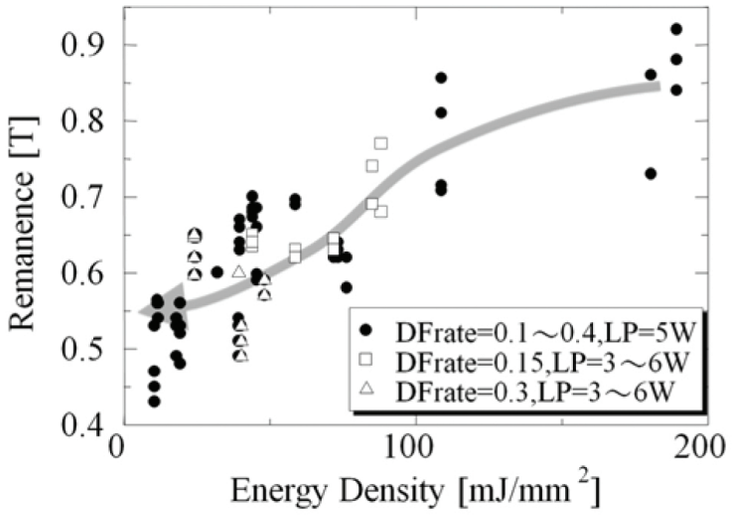

(b) Remanence

Figure 4. Effects of energy density of laser beam on (a) coercivity and (b) remanence. The laser power LP and DF rate varied independently. (a) Coercivity and (b) Remanence.

3.2. Applications comprising isotropic Nd-Fe-B thick-film magnets

Several miniaturized devices comprising the above-mentioned isotropic Nd-Fe-B thick films were demonstrated [24, 25, 28]. **Figure 5(a)** shows a small DC brushless motor with a 200-μm-thick isotropic PLD-made Nd-Fe-B film magnet. The values of coercivity and remanence of the film deposited on an Fe substrate were approximately 970 kA/m and 0.6 T, respectively. It

was confirmed that the motor with a thickness of 0.8 mm and diameter of 5 mm rotates at approximately 15,000 rpm under no-load test. The torque constant of 0.0236 mNm/A showed at the gap of 0.1 mm between a rotor and a stator.

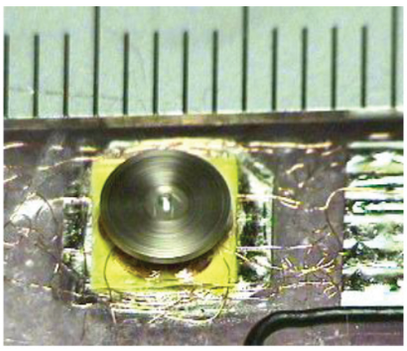

(a) DC brush-less motor

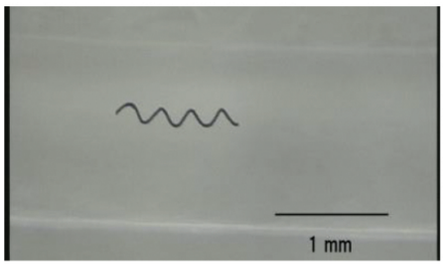

(b) Swimming machine in liquid

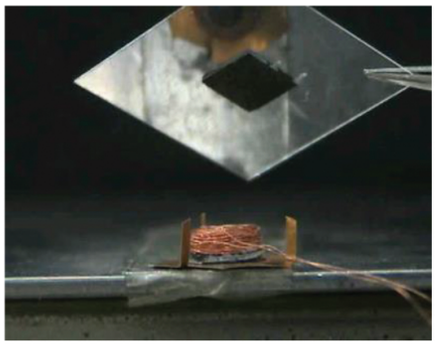

(c) Electromagnetic friction-drive micro-motor

Figure 5. Three micro-machines comprising PLD-made Nd-Fe-B thick films. (a) DC brushless motor, (b) swimming machine in liquid, and (c) electromagnetic friction-drive micro-motor.

A spiral-type micro-machine with 0.14 mm in outer diameter and 1.0 mm in length was fabricated as seen in **Figure 5(b)**. In the machine, an isotropic PLD-made Nd-Fe-B film magnet was deposited on a tungsten (W) wire. After magnetizing the film magnet in the circumferential direction, the machine rotated in sync with the rotating external magnetic field and the

spiral structure generated the propellant force. In the experiment, three types of liquids with kinematic viscosity of 1, 10, and 100 mm^2/s, respectively, were used. In order to move the wireless micro-machine, an external magnetic field of 8 kA/m was applied under the frequency range between 2 and 10 Hz. It was confirmed that the machine swam at the speed of 0.2–1.6 mm/s under various conditions.

A micro-motor using a PLD-made Nd-Fe-B film magnet with a thickness of 384 μm deposited on a Ta substrate was demonstrated as shown in **Figure 5(c)**. The stator is a coil with a ferrite core in the center together with a ferrite disc at the bottom. As an alternating voltage was applied to the coil, pulling and reacting forces worked alternatively between the film and the ferrite core, and as a result the rotor of the film magnet vibrated. The rotor is magnetically mounted onto the stator without mechanical attachments. The motor rotated at approximately 300 rpm with a starting torque of approximately 2 μNm. We confirmed that the electromagnetic friction-drive motor had a large torque together with a low rotational speed.

3.3. Isotropic Nd-Fe-B thick-film magnets deposited on Si substrates

As mentioned earlier, increase in thickness of an Nd-Fe-B film magnet is indispensable to provide a sufficient magnetic field. Here, the deposition of isotropic Nd-Fe-B thick-film magnet on Si substrates was carried out in order to apply the film magnet to various MEMS. It is generally known that we had difficulty in suppressing the peeling phenomenon due to the different values of a linear expansion coefficient for a Si substrate and an Nd-Fe-B film. Even if a buffer layer such as a Ta film was used, the maximum thickness was less than 200 μm. Here, we reported that a control of microstructure of Nd-Fe-B thick films enabled us to increase the thickness above 100 μm without a buffer layer on Si substrates [30].

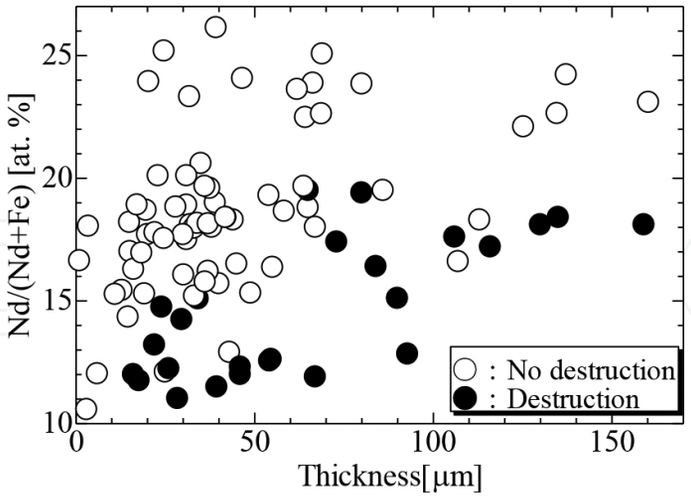

Figure 6. Relationship between thickness and Nd contents in isotropic Nd-Fe-B thick-film magnets deposited on Si substrates after an annealing process. Increase in Nd contents enabled us to increase the thickness up to 160 μm without mechanical destruction.

We investigated the relationship between thickness and Nd contents in annealed isotropic Nd-Fe-B thick films deposited on SiO_2/Si substrates as seen in **Figure 6**. After all the samples were

annealed using PA method, many samples displayed by the symbol "○" could be prepared without mechanical destruction. All the other samples plotted as "●" were broken. As the Nd content exceeded by approximately 22 at.%, the thickness of the sample symbolized "○" could be enhanced up to approximately 160 μm. The thickness of Nd-Fe-B films deposited on Si substrates increased without the deterioration of mechanical properties. It was considered that the precipitation of Nd element at the boundary of Nd-Fe-B grains together with the triple junctions due to the composition adjustment of $Nd_2Fe_{14}B$ phase is effective to suppress the destruction of the samples through an annealing process.

3.4. Isotropic Pr-Fe-B thick-film magnets deposited on glass substrates

The laser beam was focused on the surface of a $Pr_XFe_{14}B$ (X = 1.8–2.4) target under a high deposition rate of approximately several tens of microns per hour (see **Figure 1(b)**). **Figure 7** shows the magnetic properties as a function of Pr contents in each film with a thickness above 10 μm. Coercivity increased and residual magnetic polarization decreased with an increase in the amount of Pr. As displayed in **Figure 6**, Nd(or Pr)-Fe-B thick films with rare-earth amount less than 15 at.% deposited on Si substrates were mechanically broken after a post-annealing process. On glass substrates, the Pr amounts could be reduced down to approximately 13 at.% without the deterioration of mechanical properties. It was also confirmed that an approximately 100-μm-thick Pr-Fe-B thick film with $(BH)_{max}$ of about 80 kJ/m^3 could be deposited on a glass substrate.

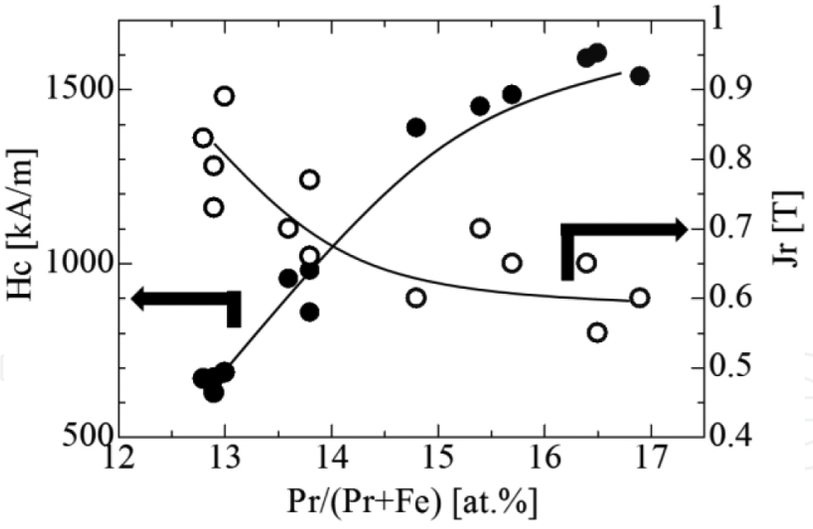

Figure 7. Remanence and coercivity as a function of Pr contents in Pr-Fe-B thick-film magnets deposited on glass substrates.

3.5. PLD-fabricated isotropic Sm-Co thick-film magnets

In this section, a high-speed PLD method with a deposition rate of approximately several tens of microns per hour was applied to fabricate Sm-Co thick-film magnets by using an $Sm_{1.2}Co_5$ target. In-plane and perpendicular M-H loops of a sample annealed by CA method are shown

http://dx.doi.org/10.5772/64235

in **Figure 8**. The perpendicular M-H loop was corrected by a demagnetization factor of 1.0. The structure of as-deposited films prepared using an $SmCo_5$ target without a substrate heating system was amorphous as seen in **Figure 9**; therefore, the samples were post-annealed at a temperature of 973 K with a heating rate of 673 K/min (CA method). After the post annealing, not only $SmCo_5$ but also Sm_2Co_{17} phases were observed. In the present stage, we demonstrate the fabrication nano-composite Sm-Co/α-Fe multilayered film magnets using the PLD method [31].

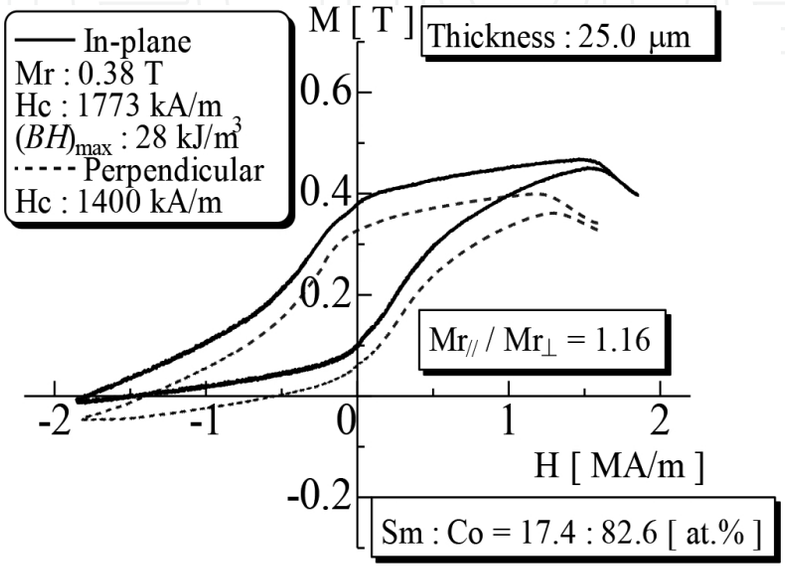

Figure 8. In-plane and perpendicular M-H loops of a PLD-fabricated Sm-Co thick film after a post-annealing process.

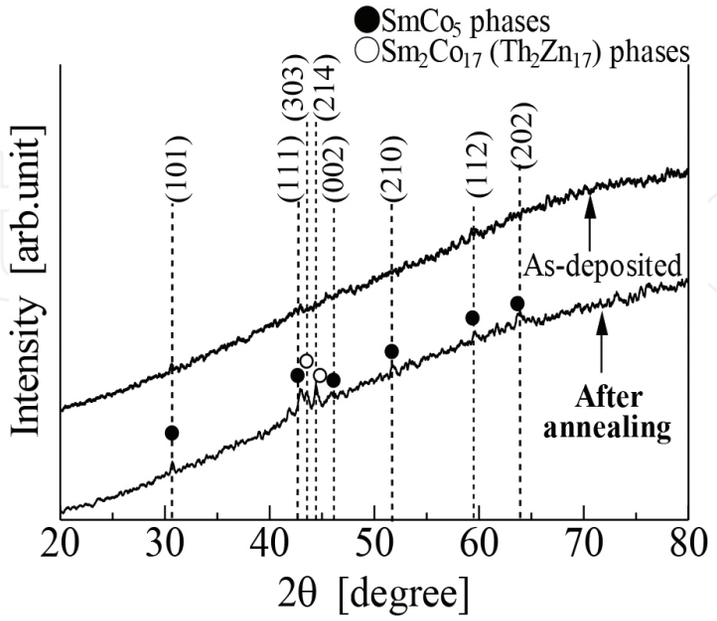

Figure 9. X-ray diffraction patterns of a PLD-fabricated Sm-Co thick film before and after a post-annealing process.

3.6. PLD-fabricated isotropic Fe-Pt thick-film magnets

In this section, a $Fe_{70}Pt_{30}$ target was ablated with an Nd-YAG pulse laser under LED above 200 mJ/mm^2 in a vacuum atmosphere (see **Figure 1(a)**). **Figure 10** shows coercivity values of the as-deposited films as a function of laser power. The values drastically increased at a power of 3 W and then gradually decreased with increase in power. We confirmed that the substrate temperature was proportional to the laser power due to the rise of a radiation heat from a target. As a result, it was found that $L1_0$ ordered phase together with relatively high coercivity could be obtained using a suitable laser power without using a substrate heating system and a post-annealing process. **Figure 11** shows in-plane M-H loop of a Fe-Pt film fabricated at a power of 3 W. The values of coercivity, remanence, and $(BH)_{max}$ were 378 kA/m, 0.94 T, and 104 kJ/m^3, respectively [32]. We, therefore, considered that remanence enhancement occurred in the sample because the saturation magnetization of 1.43 T for $Fe_{50}Pt_{50}$ ordered phase [33].

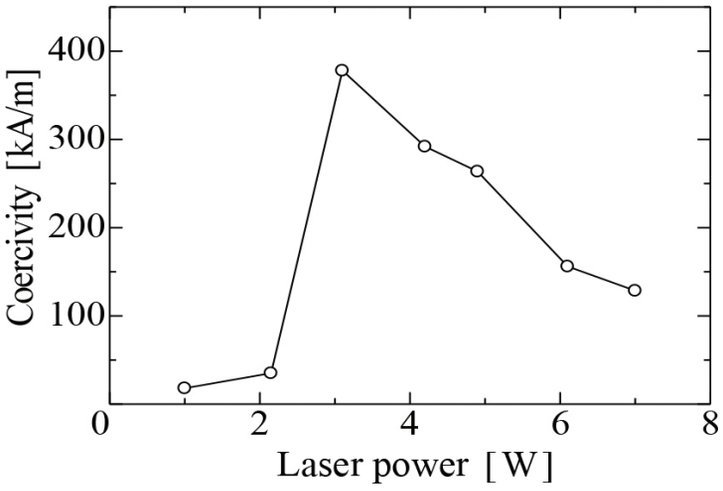

Figure 10. In-plane coercivity values for as-deposited Fe-Pt film magnets prepared from $Fe_{70}Pt_{30}$ target as a function of laser power.

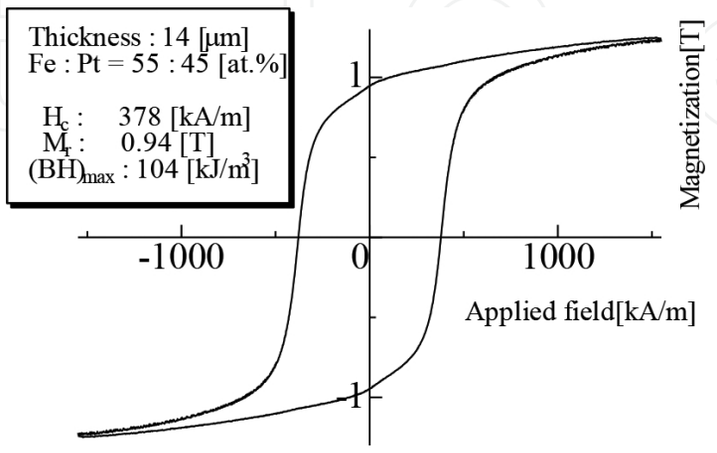

Figure 11. In-plane and perpendicular M-H loops of an as-deposited Fe-Pt film magnet prepared from a $Fe_{70}Pt_{30}$ target.

http://dx.doi.org/10.5772/64235

3.7. PLD-fabricated isotropic nano-composite Nd-Fe-B + α-Fe thick-film magnets

In this section, we focus on the use of high LED above 200 mJ/mm^2 in order to adopt a different deposition process by taking account of the explosively emitting process of atoms from a target. The as-deposited films had amorphous phase including α-Fe grains, and a nano-composite structure could be obtained after the pulse annealing [34].

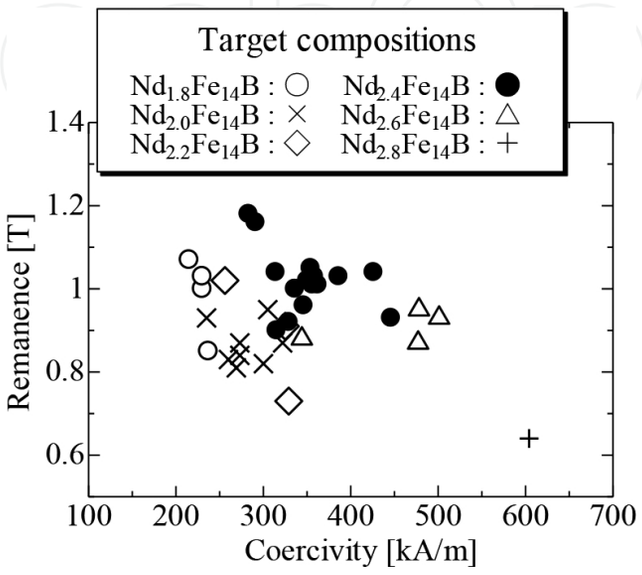

Figure 12. Relationship between remanence and coercivity values of films thicker than 10 μm by using six targets with various compositions. Use of an $Nd_{2.4}Fe_{14}B$ target is effective to obtain good magnetic properties.

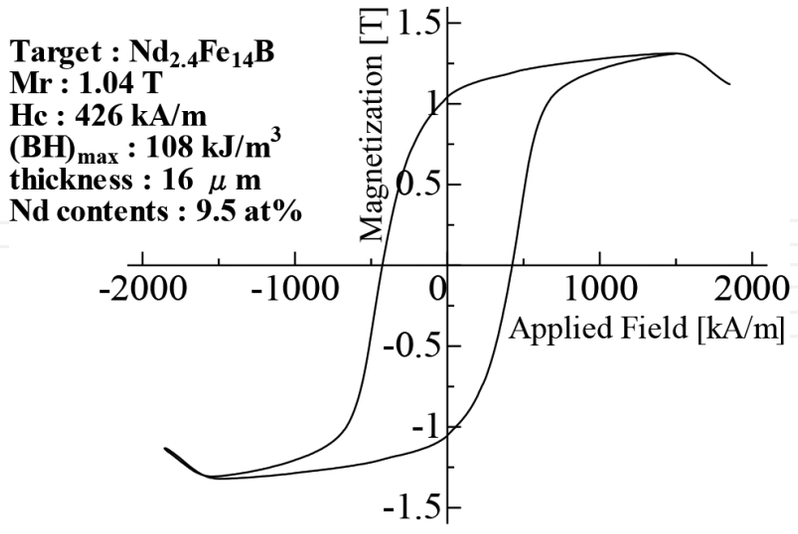

Figure 13. M-H loop of a 16-μm-thick Nd-Fe-B film magnet prepared using laser energy density above 200 mJ/mm^2 together with an $Nd_{2.4}Fe_{14}B$ target.

Investigation on the relationship between coercivity and remanence of each sample thicker than 10 μm prepared by six Nd-Fe-B targets with various compositions under LED above

200 mJ/mm^2 (see **Figure 12**). In all the targets, the deposition rate was higher than 20 μm/h and the reduction in the Nd contents of each film by several atomic percentages was observed compared with that of the corresponding target. The samples prepared by using an $Nd_{2.4}Fe_{14}B$ target had relatively large values of coercivity and remanence. **Figure 13** shows an in-plane M-H loop of a 16-μm-thick Nd-Fe-B + α-Fe thick-film magnet prepared using LED higher than 200 mJ/mm^2 together with an $Nd_{2.4}Fe_{14}B$ target.

4. Conclusion

In this chapter, we introduced the preparation of rare-earth thick-film magnets using a PLD method and their applications. The PLD-made Nd-Fe-B thick-film magnets thicker than 10 μm deposited on metal substrates could be applicable to miniaturized devices by taking account of the relatively good magnetic and mechanical properties. In addition, Nd(or Pr)-Fe-B thick films with a thickness above 100 μm without a buffer layer on a Si or glass substrate. Preparation of Sm-Co, Fe-Pt, and nano-composite Nd-Fe-B + α-Fe thick-film magnets was also carried out.

Author details

Masaki Nakano*, Takeshi Yanai and Hirotoshi Fukunaga

*Address all correspondence to: mnakano@nagasaki-u.ac.jp

Graduate School of Engineering, Nagasaki University, Nagasaki, Japan

References

[1] F. Dumas-Bouchat, L. F. Zanini, M. Kustov, N. M. Dempsey, R. Grechishkin, K. Hasselbach, J. C. Orlianges, C. Champeaux, A. Catherinot, and D. Givord, *Appl. Phys. Lett*. 96, 102511 (2010).

[2] A. Walther, C. Marcoux, B. Desloges, R. Grechishkin, D. Givord, and N. M. Dempsey, *J. Magn. Magn. Mater*. 321, 590 (2009).

[3] N. M. Dempsey, A. Walther, F. May, D. Givord, K. Khlopkov, and O.Gutfleisch, *Appl. Phys. Lett*. 90, 092509 (2007).

[4] M. Uehara, *J. Magn. Magn. Mater*. 284, 281 (2004).

[5] L. K. B. Serrona, A. Sugimura, N. Adachi, T. Okuda, H. Ohsato, I. Sakamoto, A. Nakanishi, M. Motokawa, D. H. Ping, and K. Hono, *Appl. Phys. Lett*. 82, 1751 (2003).

[6] B. A. Kapitanov, N. V. Kornilov, Ya. L. Linetsky, and V. Yu. Tsvetkov, *J. Magn. Magn. Mater*. 127, 289 (1993).

[7] S. Yamashita, J. Yamasaki, M. Ikeda, and N. Iwabuchi, *J. Appl. Phys*. 70, 6627 (1991).

[8] T. Spelitos, D. Niarchos, V. Skumryev, Y. Zhang, and G. Hadjipanayis, *J. Magn. Magn. Mater*. 272–276, e877(2004).

[9] A. Melsheimer, and H. Kronműller, *Phys. B*. 299, 251 (2001).

[10] J. Töpfer, B. Pawlowski, and B. Pawlowski, *Proceedings of the 18th Int. Workshop on High Performance Magnets and Their Applications*, 828 (2004).

[11] F. Yamashita, S. Nishimura, N. Menjo, O. Kobayashi, M. Nakano, H. Fukunaga, and K. Ishiyama, *IEEE Trans. Magn*. 46, 2012 (2010).

[12] S. Fahler, V. Neu, U. Hannemann, S. Oswald, J. Thomas, B. Holzapfel, and L. Schultz, Annual report 2001 in IFW Dresden, 21 (2001).

[13] K. Chen, H. Hegde, S. U. Jen, and F. J. Cadieu, *J. Appl. Phys*. 73, 5923 (1999).

[14] S. Takei, X. Liu, and A. Morisako, *Phys. Stat. Sol.(a)* 204, 12, 4166(2007).

[15] L. N. Zhang, J. S. Chen, J. Ding, and J. F. Hu, *J. Appl. Phys*. 103, 043911 (2008).

[16] F. J. Cadieu, H. Hegde, E. Schloemann, and H. J. Van Hook, *J. Appl. Phys*. 76, 6059 (1994).

[17] F. J. Cadieu, R. Rani, X. R. Qian, and Li Chen, *J. Appl. Phys*. 83, 6247 (1998).

[18] F. J. Cadieu, R. Rani, T. Theodoropoulos, and Li Chen, *J. Appl. Phys*. 85, 5895 (1999).

[19] T. Budde, and Hans H. Gatzen, *J. Appl. Phys*. 99, 08N304 (2006).

[20] T. Nakayama, M. Watanabe, M. Homma, T. Kanno, K. Kimura, and O. Okuno, *J. Magn. Soc. Jpn*. 21, 377 (1997). (in Japanese).

[21] A. Yamazaki, M. Sendoh, K. Ishiyama, K. I. Arai, R. Kato, M. Nakano, and H. Fukunaga, *J. Magn.Magn. Mater*. 272–276, e1741 (2004).

[22] H. Aoyama, and Y. Honkura, *J. Magn. Soc. Jpn*. 20, 237 (1996). (in Japanese).

[23] W. F. Liu, S. Suzuki, D. S. Li, and K. Machida, *J. Magn. Magn. Mater*. 302, 201 (2006).

[24] M. Nakano, S. Sato, H. Fukunaga and F. Yamashita, *J. Appl. Phys*. 99, 08N301 (2006).

[25] M. Nakano, S. Sato, F. Yamashita, T. Honda, J. Yamasaki, K. Ishiyama, M. Itakura, J. Fidler, T. Yanai, and H. Fukunaga, *IEEE Trans. Magn*. 43, 2672 (2007).

[26] M. Nakano, H. Takeda, F. Yamashita, T. Yanai, and H. Fukunaga, *IEEE Trans. Magn*. 44, 4229 (2008).

[27] H. Fukunaga, T. Kamikawatoko, M. Nakano, T. Yanai, and F. Yamashita, *J. Appl. Phys*. 109, 07A758 (2011).

[28] M. Nakano, T. Honda, J. Yamasaki, S. Sato, F. Yamashita, J. Fidler, and H. Fukunaga, *Sens. Lett*. 5, 48 (2007).

[29] M. Nakano, S. Tsutsumi, and H. Fukunaga, *IEEE Trans. Magn*. 38, 2913 (2002).

[30] M. Nakano, Y. Chikuba, M. Oryoshi, A. Yamashita, T. Yanai, R. Fujiwara, T. Shinshi, and H. Fukunaga, *IEEE Trans. Magn*. 51, #2102604 (2015).

[31] H. Fukunaga, A. Tou, M. Itakura, M. Nakano, and T. Yanai, *IEEE Trans. Magn*. 50, 2101504 (2014).

[32] M. Nakano, W. Oniki, T. Yanai, and H. Fukunaga, *J. Appl. Phys*. 109, 07A723 (2011).

[33] O. Gutfleisch, J. Lyubina, K. H. Műller, and L. Schultz, *Adv. Eng. Mater*. 7, 208 (2005).

[34] M. Nakano, K. Motomura, T. Yanai, and H. Fukunaga, *IEEE Trans. Magn*. 50, 2101404 (2014).